Generalized Analysis of Stability and Numerical Dispersion in the Discrete-Convolution FDTD Method

William A. Beck, *Member, IEEE,* and Mark S. Mirotznik, *Member, IEEE*

***Abstract*—A simple technique is described for determining the stability and numerical dispersion of finite-difference time-domain (FDTD) calculations that are linear, second-order in space and time, and include dispersion by the discrete convolution method. The technique is applicable to anisotropic materials. Numerical examples demonstrate the accuracy of the technique for several anisotropic and/or dispersive materials.**

***Index Terms*—FDTD methods, numerical dispersion, stability analysis.**

I. Introduction

In 1966, Yee [1] introduced the finite-difference time-domain (FDTD) method using the leapfrog approximation of Maxwell's two time-dependent curl equations for isotropic lossless materials. Since then, the method has been extended to materials that are lossy, anisotropic, and dispersive [2], [3] and has been extensively used to solve a wide range of practical problems.

Two important issues for all FDTD calculations are numerical dispersion and stability. Numerical dispersion is introduced by the discretization of Maxwell's equations and causes electromagnetic waves to propagate with different wavelength and attenuation in the FDTD grid than in continuous space. It also results in anisotropic propagation, even when the material properties are isotropic. Stability analysis is necessary because the FDTD algorithms are only conditionally stable. They typically converge when the time step is smaller than some critical value, but diverge exponentially for larger time steps.

The original FDTD technique has given rise to many variations, introduced to include loss, dispersion, and nonlinear material properties as well as to improve accuracy and/or stability for particular types of materials. However, there are now so many variations that a fully general analysis of dispersion and stability may not be possible. We focus our analysis here on FDTD procedures that are linear, use second-order finite differences and include dispersion by the method of discrete convolution [3], [4]. Such FDTD programs are widespread, for example in the commercial program XFDTD [5].

The numerical dispersion and stability of the original FDTD procedure for lossless nondispersive materials are well known [2], [3]. Others have studied numerical dispersion and stability in lossy dielectrics [6] and dispersive dielectrics [7]–[12]. Weedon and Rappaport [10] implemented a general analysis of dispersion and stability using a Padé approximation for the frequency-dependent permittivity or conductivity. Their procedure can be used to form a finite-difference approximation for arbitrary dispersive properties obtained from measured data if enough terms are included. Also, the coefficients of the Padé approximation can be chosen to partially emulate other methods, including the discrete convolution method. However, their method is not applicable to the complex discrete convolution used to describe Lorentz dispersion [4] (although their method can be used to treat Lorentz materials modeled using differential equation-based methods).

In this paper, we present a technique for determining numerical dispersion by simple substitution into the continuous (nonnumerical) dispersion relation. The procedure is applicable to all anisotropic and dispersive materials whose dispersion is simulated by discrete convolution. We then present a simple technique for evaluating stability using the numerical dispersion relation. Several numerical examples are presented to demonstrate the accuracy of the techniques.

II. Analysis

A. Continuous Dispersion

Using meter-kilogram-second-ampere (MKSA) units, the Maxwell curl equations that are solved by the FDTD procedure are

$$\partial_t \mathbf{B} = \mu_0[1+\psi(\omega)]\partial_t \mathbf{H} = -\nabla \times \mathbf{E} - \eta \cdot \mathbf{H} \tag{1}$$

$$\partial_t \mathbf{D} = \varepsilon_0[1+\chi(\omega)]\partial_t \mathbf{E} = \nabla \times \mathbf{H} - \sigma \cdot \mathbf{E} \tag{2}$$

where ∂_T indicates the partial derivative with respect to time, ω is the angular frequency, $\mathbf{E}$ is the electric field, $\mathbf{H}$ is the magnetic field, $\mathbf{D}$ is the electric flux density, $\mathbf{B}$ is the magnetic flux density, $\chi(\omega)$ and $\psi(\omega)$ are electric and magnetic susceptibilities, respectively, σ is the conductivity, and η is an equivalent magnetic resistivity. The material properties $\chi(\omega), \psi(\omega), \eta$, and σ may be tensors in the case of anisotropic materials. Both η and σ are assumed to be independent of ω.

To determine the dispersion relation, we consider harmonic plane wave solutions of the form

$$\mathbf{V} = \mathbf{V}_0 \exp[j(\omega t - \mathbf{k} \cdot \mathbf{r})] \tag{3}$$

Manuscript received April 23, 1999; revised January 11, 2000.

W. A. Beck is with the U.S. Army Research Laboratory, Adelphi, MD 20783 USA.

M. S. Mirotznik is with the Department of Electrical Engineering, Catholic University of America, Washington, DC 20064 USA.

Publisher Item Identifier S 0018-926X(00)05801-4.

where $\mathbf{V}$ represents $\mathbf{E}$ or $\mathbf{H}$, $\mathbf{k}$ is the propagation vector, $\mathbf{r}$ is the position, and t is the time. In this case, (1) and (2) can be written as

$$\omega\hat{\mu}(\omega)\mathbf{H}_0 = (\mathbf{k}\times\mathbf{E}_0) \tag{4}$$

$$\omega\hat{\varepsilon}(\omega)\mathbf{E}_0 = -(\mathbf{k}\times\mathbf{H}_0) \tag{5}$$

where

$$\hat{\mu}(\omega) = \mu_0[1+\psi(\omega)] - \frac{j\eta}{\omega} \tag{6}$$

$$\hat{\varepsilon}(\omega) = \varepsilon_0[1+\chi(\omega)] - \frac{j\sigma}{\omega} \tag{7}$$

are the complex permeability and permittivity, respectively. Both $\hat{\mu}$ and $\hat{\varepsilon}$ may be tensors. Equations (4) and (5) can then be solved for the continuous dispersion relation $\omega(\mathbf{k})$.

For isotropic material properties, the continuous dispersion is the scalar equation

$$\hat{\varepsilon}(\omega)\hat{\mu}(\omega)\omega^2 = k^2. \tag{8}$$

For anisotropic (nonmagnetic) dielectrics, the three-dimensional (3-D) dispersion is the solution of the determinant equation [13] in (9), shown at the bottom of the page.

Solutions are also available for anisotropic magnetic properties. Although the result may be complicated, the continuous dispersion relation is generally already known for the materials being simulated in an FDTD problem.

B. Numerical Dispersion Analysis

Consider how the continuous dispersion is altered by the approximations made in the FDTD procedure. Three approximations are used in the common version of FDTD that we have analyzed: replacement of continuous derivatives by finite differences, evaluation of $\eta\cdot\mathbf{H}$ and $\sigma\cdot\mathbf{E}$ in (1) and (2) at shifted times, and replacement of the frequency-dependent susceptibilities by discrete convolutions in the time domain. We consider each of these in turn.

In the following discussion, Δ_t is the full time step between successive values of $\mathbf{E}$ (or $\mathbf{H}$) and Δ_β is the full spatial step in the β direction ($\beta = x, y, z$). Where both primed and unprimed variables are used, the primed and unprimed versions are to be used in the numerical and continuous dispersion relations, respectively.

1) Use of Finite Differences: Let δ_β indicate the finite-difference operator $\delta_\beta f_n = (f_{n+1/2} - f_{n-1/2})/\Delta_\beta$, where Δ_β is the step size for the spatial variable β and similarly let $\delta_t f_m = (f_{m+1/2} - f_{m-1/2})/\Delta_t$. Also let $\delta\times$ indicate the finite-difference curl operator obtained from the continuous curl operator by replacement of each of the derivatives with respect to coordinate β by δ_β. Using this notation, it is easy to show that the continuous relations $\partial_t\mathbf{V} = j\omega\mathbf{V}$ and $\nabla\times\mathbf{V} = -j(\mathbf{k}\times\mathbf{V})$ transform into the finite-difference expressions $\delta_t\mathbf{V} = j\omega\ \mathrm{sinc}\ (\theta_t)\mathbf{V}$ and $\delta\times\mathbf{V} = -j(\vec{\kappa}\times\mathbf{V})$, respectively, where $\kappa_\beta = k_\beta\ \mathrm{sinc}\ (\theta_\beta), \theta_t = \omega\Delta_t/2, \theta_\beta = k_\beta\Delta_\beta/2$, and $\mathrm{sinc}(x) = \sin(x)/x$. Use of these finite-difference operators in (1) and (2) is equivalent to replacing $\mathbf{k}$ in (4) and (5) by $\mathbf{k}'$, whose components are

$$k'_\beta - k_\beta\ \mathrm{sinc}\ (\theta_\beta)/\mathrm{sinc}\ (\theta_t). \tag{10}$$

2) Time Shifting of $\eta\cdot\mathbf{H}$ and $\sigma\cdot\mathbf{E}$: Time shifting of $\eta\cdot\mathbf{H}$ and $\sigma\cdot\mathbf{E}$ is needed since a straightforward discretization of (1) and (2) does not yield proper time staggering of $\mathbf{E}$ and $\mathbf{H}$. Therefore, these fields must be replaced by some combination of properly staggered fields. Letting $\mathbf{E}^n$ represent the electric field at time step n, Taflove [2] proposed using the average of $\mathbf{E}^{n+1}$ and $\mathbf{E}^n$ as a reasonable estimate of $\mathbf{E}^{n+1/2}$. On the other hand, Kunz and Luebbers [3] proposed using $\mathbf{E}^{n+1}$ to improve stability when lossy materials are used. Like Perada *et al.* [6], we refer to these as the time-average (TA) and time-forward (TF) approaches, respectively. It can be shown that the effect of the time shifting is equivalent to replacing η and σ by $\eta' = \eta g(\theta_t)$ and $\sigma' = \sigma g(\theta_t)$, respectively, with $g(\theta_t)$ defined for the two approaches as

$$g(\theta_t) = \begin{cases} \dfrac{\exp(j\theta_t)}{\mathrm{sinc}(\theta_t)}, & \text{(TF)} \\ \dfrac{\cos(\theta_t)}{\mathrm{sinc}(\theta_t)}, & \text{(TA).} \end{cases} \tag{11}$$

3) Use of Discrete Convolution: Finally, the frequency-domain susceptibilities $\chi(\omega)$ and $\psi(\omega)$ are replaced by discrete time-domain convolutions, $\chi'(\omega)$ and $\psi'(\omega)$, given by [3]

$$\chi(\omega) = \int_0^\infty \chi(\tau)\exp(-j\omega\tau)\,d\tau$$

$$\rightarrow \chi'(\omega) = \sum_{m=0}^{\infty} \exp(-j\omega\Delta_t m)\chi_m \tag{12}$$

with

$$\chi_m = \int_{m\Delta_t}^{(m+1)\Delta_t} \chi(t)\,dt \tag{13}$$

and the analogous forms for $\psi'(\omega)$. In many cases (including the important cases of Debye, Drude, and Lorentz dispersion), χ_m can be expressed in the recursive form [3]

$$\chi_m = \mathrm{Re}\ [\hat{G}\exp(-\hat{v}m\Delta_t)]. \tag{14}$$

where Re indicates the real part, $\hat{G}$ is a complex function that depends on Δ_t, but not on m and $\hat{v}$ is a complex frequency. In

$$0 = \begin{vmatrix} \omega^2\mu_0\hat{\varepsilon}_{xx} - k_y^2 - k_z^2 & \omega^2\mu_0\hat{\varepsilon}_{xy} + k_xk_y & \omega^2\mu_0\hat{\varepsilon}_{xz} + k_xk_z \\ \omega^2\mu_0\hat{\varepsilon}_{yx} + k_xk_y & \omega^2\mu_0\hat{\varepsilon}_{yy} - k_x^2 - k_z^2 & \omega^2\mu_0\hat{\varepsilon}_{yz} + k_yk_z \\ \omega^2\mu_0\hat{\varepsilon}_{zx} + k_xk_z & \omega^2\mu_0\hat{\varepsilon}_{zy} - k_yk_z & \omega^2\mu_0\hat{\varepsilon}_{zz} - k_x^2 - k_y^2 \end{vmatrix} \tag{9}$$

these cases, we can evaluate the sum in (12) to obtain the explicit form

$$\chi'(\omega) = \frac{1}{2}\left[\frac{\hat{G}}{1-\exp[-(j\omega+\hat{v})\Delta_t]} + \frac{\hat{G}^*}{1-\exp[-(j\omega+\hat{v}^*)\Delta_t]}\right] \tag{15}$$

where $*$ indicates complex conjugation. A similar procedure yields an analogous expression for $\psi'(\omega)$.

4) Net Effect on Numerical Dispersion: Incorporating all three of the approximations, the discrete versions of (4) and (5) are

$$\omega\hat{\mu}'(\omega)\mathbf{H}_0 = (\mathbf{k}'\times\mathbf{E}_0) \tag{16}$$

$$\omega\hat{\varepsilon}'(\omega)\mathbf{E}_0 = -(\mathbf{k}'\times\mathbf{H}_0) \tag{17}$$

with

$$\hat{\mu}'(\omega) = \mu_0[1+\psi'(\omega)] - \frac{j\eta g(\theta_t)}{\omega} \tag{18}$$

$$\hat{\varepsilon}'(\omega) = \varepsilon_0[1+\chi'(\omega)] - \frac{j\sigma g(\theta_t)}{\omega}. \tag{19}$$

Note that the discrete equations (16) and (17) have exactly the same form as the continuous equations (4) and (5), except for the modified parameters $\hat{\mu}'(\omega), \hat{\varepsilon}'(\omega)$, and $\mathbf{k}'$.

Therefore, to determine the numerical dispersion relation, we first evaluate the numerical susceptibility using (15) if the dispersion can be written in the recursive form (14) or, otherwise, by numerically evaluating the sum in (12). If either $\hat{\mu}(\omega)$ or $\hat{\varepsilon}(\omega)$ are tensors, we perform the appropriate substitution for each of the components. We then substitute the modified $\hat{\mu}'(\omega), \hat{\varepsilon}'(\omega)$, and $\mathbf{k}'$ into the continuous dispersion relation (e.g., (8) for an isotropic material or (9) for an anisotropic dielectric) to obtain the numerical dispersion relation. This substitution method permits evaluation of numerical dispersion even for complicated materials with dispersive anisotropic properties.

For isotropic material properties, the numerical version of (8) is again a scalar equation that can be written as

$$\hat{n}'^2(\omega)\omega^2 = c^2k'^2 \tag{20}$$

where $\hat{n}'(\omega)$ is the complex numerical refractive index defined by

$$\hat{n}'^2(\omega) = \hat{\varepsilon}'(\omega)\hat{\mu}'(\omega)/\varepsilon_0\mu_0 \tag{21}$$

and c is the speed of light.

When $\chi'(\omega)$ and $\psi'(\omega)$ are generated by *recursive* discrete convolution, so that (15) applies, the function $\hat{n}'^2(\omega)$ has two interesting properties that will be useful for stability analysis. First, it can be shown that $\hat{\mu}'(\omega)$ and $\hat{\varepsilon}'(\omega)$ are both real at the temporal Nyquist frequency $\omega_{Ny} = \pi/\Delta_t$ and so $\hat{n}'^2(\omega_{Ny})$ is also real. Second, $\hat{\mu}'(\omega)$ and $\hat{\varepsilon}'(\omega)$ are both conjugate-symmetric around ω_{Ny}, i.e., $\hat{\varepsilon}'(\omega_{Ny}+\omega) = \hat{\varepsilon}'^*(\omega_{Ny}-\omega)$ and so $\hat{n}'^2(\omega)$ is also conjugate-symmetric around ω_{Ny}.

It is interesting that the three approximations used in the FDTD procedure are each associated with a different time or length scale. First, replacement of continuous space and time derivatives with finite differences leads to the modified $\mathbf{k}'$, whose deviation from $\mathbf{k}$ is determined by $\omega\Delta_t$ and $k_\beta\Delta_\beta$. This results in a simple (direction-dependent) scaling of the dispersion relation along the k-axis, but no change in the spectral shape. Second, the use of time-shifted fields to evaluate the loss terms in (1) and (2) leads to scaling of η and σ by $g(\theta_t)$, again determined by $\omega\Delta_t$. As shown elsewhere [6], the associated error in the real part of $\hat{\varepsilon}(\omega)$ is proportional to $\omega\tau_\sigma$, where $\tau_\sigma = \varepsilon/\sigma$ is the relaxation time of the medium. Third, approximation of $\chi(\omega)$ and $\psi(\omega)$ by discrete convolutions leads to the modified values in (15), with the deviation determined by both $\omega\Delta_t$ and $\hat{v}\Delta_t$. Both the second and third effects change the spectral shape of the dispersion relation. Therefore, to accurately represent the problem, the spatial steps Δ_β must be small compared to $1/k$ and the time step Δ_t must be small compared to all three time scales, $1/\omega$, τ_σ, and $1/|\hat{v}|$.

C. General Stability Analysis

Consider a region of FDTD grid that is homogeneously filled with a possibly dispersive and anisotropic material. The instantaneous fields at any time t in that region can be written as a Fourier sum over the normal modes of the grid, which are plane waves with *real* $\mathbf{k}$ and with $|k_\beta| \le 2\pi/\Delta_\beta$. Note that because of the spatial interleaving of $\mathbf{E}$ and $\mathbf{H}$, the maximum k_β is the spatial Nyquist frequency corresponding to a spacing of $\Delta_\beta/2$ and is twice the Nyquist frequency for the individual $\mathbf{E}$ and $\mathbf{H}$ fields. Similarly, the maximum temporal frequency is $2\pi/\Delta_t$, corresponding to twice the temporal Nyquist frequency for the individual fields.

Since the numerical dispersion relation yields $\omega(\mathbf{k})$ for any $\mathbf{k}$-mode of the FDTD grid, the problem will be absolutely stable if and only if $\mathrm{Im}[\omega(\mathbf{k})] \le 0$ for all normal modes. Otherwise, numerical noise due to finite precision arithmetic will eventually excite any $\mathbf{k}$-mode associated with $\mathrm{Im}[\omega(\mathbf{k})] > 0$ and the mode will grow without limit.

1) Stability for Isotropic Materials: Consider isotropic material properties. We first present a graphical treatment using stability diagrams to show the mathematical basis of the analysis. Based on this analysis, we then present a simple set of rules for evaluating stability.

It is convenient to define the normalized scalar variable

$$\hat{\kappa}^2 = \sum_{\beta=1}^{N}\frac{\sin^2(\theta_\beta)}{\Delta_\beta^2}\Bigg/\sum_{\beta=1}^{N}\frac{1}{\Delta_\beta^2} \tag{22}$$

where N is the dimensionality of the problem and also the function

$$f(\omega) = \sin^2\left(\frac{\omega\Delta_t}{2}\right)\left[\frac{1}{c^2\Delta_t^2}\Bigg/\sum_{\beta=1}^{N}\frac{1}{\Delta_\beta^2}\right] \tag{23}$$

so that we can rewrite (20) as

$$\hat{n}'^2(\omega)f(\omega) = \hat{\kappa}^2(\omega). \tag{24}$$

Equation (24) can be viewed as a transformation between the complex plane of ω values and the complex plane of $\hat{\kappa}^2$ values. The upper half of the ω-plane represents unstable solutions; the lower half and the real axis represent stable solutions. In the

$\hat{\kappa}^2$-plane, the normal modes of the grid fall along a line segment on the real axis with $0 \leq \hat{\kappa}^2 \leq 1$.

To evaluate stability, we map the unstable upper half of the ω-plane into the $\hat{\kappa}^2$-plane. We obtain the boundary of this region by mapping the real-ω axis into the $\hat{\kappa}^2$-plane. We need only consider $0 \leq \omega \leq 2\omega_{Ny}$, which maps to a closed loop in the $\hat{\kappa}^2$-plane, beginning at the origin, crossing the real-$\hat{\kappa}^2$ axis when $\omega = \omega_{Ny}$, and returning to the origin when $\omega = 2\omega_{Ny}$. The values of $\hat{\kappa}^2$ inside the closed loop correspond to stable solutions, while those outside the loop are unstable. The FDTD problem will be absolutely stable if, and only if, all normal modes of the grid lie inside the stability loop.

For a simple example, consider a Debye material with

$$\hat{\varepsilon}(\omega) = \varepsilon_\infty + \frac{\varepsilon_s - \varepsilon_\infty}{1 + j\omega\tau_c}. \tag{25}$$

Using typical parameters for water $\varepsilon_s = 81.0, \varepsilon_\infty = 1.8, \tau_c = 9.4 \times 10^{-12}$s and a cell size of 37.5 μm, the one-dimensional (1-D) Courant time step is 1.25×10^{-13} s. Fig. 1 shows the corresponding stability diagram. All normal modes are in the stable region inside the loop, so the region containing this material would be stable.

Fig. 1 illustrates two general properties of stability loops that derive from the previously mentioned symmetries of $\hat{n}'^2(\omega)$. First, since $\hat{n}'^2(\omega_{Ny})$ is real, the stability loop crosses the real axis when $\omega = \omega_{Ny}$. Second, because $\hat{n}'^2(\omega)$ and $f(\omega)$ are conjugate-symmetric and symmetric, respectively, around ω_{Ny}, the stability loop has mirror symmetry across the real-$\hat{\kappa}^2$ axis.

Fig. 2 shows a more complicated stability diagram for a Lorentz material with

$$\hat{\varepsilon}(\omega) = \frac{(\varepsilon_s - \varepsilon_\infty)}{\omega_p^2 + 2j\omega\delta_p - \omega^2} \tag{26}$$

$\omega_p = 4.0 \times 10^{16}$ Hz, $\delta_p = 0.28 \times 10^{16}$ Hz, $\varepsilon_\infty = 2.25$, and $\varepsilon_s = 1.0$, a cell size of 12 nm, and the corresponding Courant time step of 4.0×10^{-17} s. In this case, there is no stable region; the unstable upper half of the ω-plane maps to the entire $\hat{\kappa}^2$-plane. Therefore, all modes, including the normal modes of the grid, are unstable. However, as shown in Fig. 3, reducing the time step to $\sim 0.7 \times 10^{-17}$ s yields absolute stability of all normal modes.

The stability diagram is informative because it explicitly shows any overlap between the states in the unstable upper half of the ω-plane and the normal modes of the grid in the $\hat{\kappa}^2$-plane. However, we can evaluate stability at a given Δ_t by direct examination of the properties of $\hat{\kappa}^2$, without plotting the stability diagram. First note that a *necessary* condition for all normal modes of the grid to lie inside the stability loop is that $\hat{\kappa}^2(\omega_{Ny}) \geq 1$ and therefore, since $f(\omega_{Ny}) = 1, \hat{n}'^2(\omega)_{Ny} \geq 1$. We refer to this as the Nyquist stability requirement. The critical time step corresponding to this condition is called the Nyquist time step, indicated by Δ_{tNy}, which one can obtain simply by substituting the temporal and spatial Nyquist frequencies $\omega = \omega_{Ny}$ and $k_\beta = k_{\beta,Ny} = \pi/\Delta_\beta$ into the numerical dispersion relation and solving for Δ_t. It is easy to show that this yields the usual Courant value of $\Delta_t = [c\sqrt{N \, \Sigma_{\beta=1}^{N} \, (1/\Delta_\beta^2)}]^{-1}$ when $\hat{n}'(\omega) = 1$.

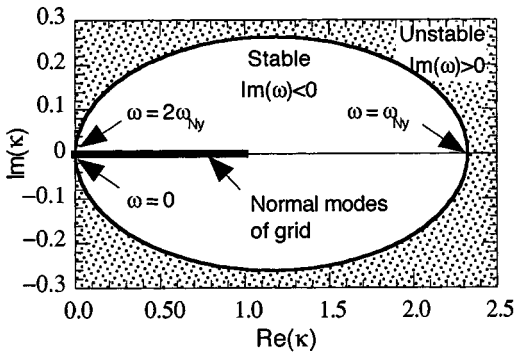

Fig. 1. Stability loop for a Debye material (water) with $\varepsilon_s = 81.0, \varepsilon_\infty = 1.8$, and $t_c = 9.4 \times 10^{-12}$ s, cell size of 37.5 μm, and Courant time step. Shaded areas are unstable. All normal modes are inside the loop, indicating that the region containing this material should be stable.

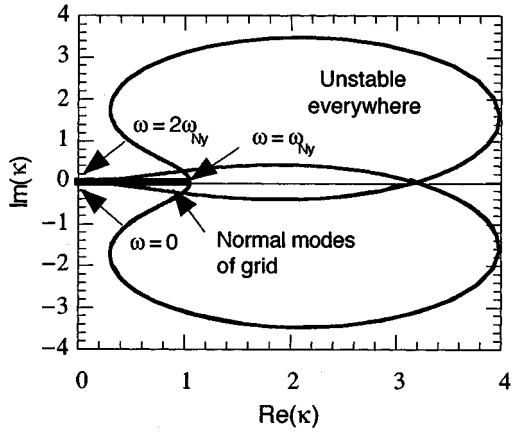

Fig. 2. Stability loop for a Lorentz material with $\omega_p = 4.0 \times 10^{16}$ Hz, $\delta_p = 0.28 \times 10^{16}$ Hz, $\varepsilon_\infty = 2.25, \varepsilon_s = 1.0$, cell size of 12 nm, and Nyquist time step. All modes are associated with $\mathrm{Im}[\hat{\varepsilon}'(\omega)] > 0$ so FDTD problem will be unstable.

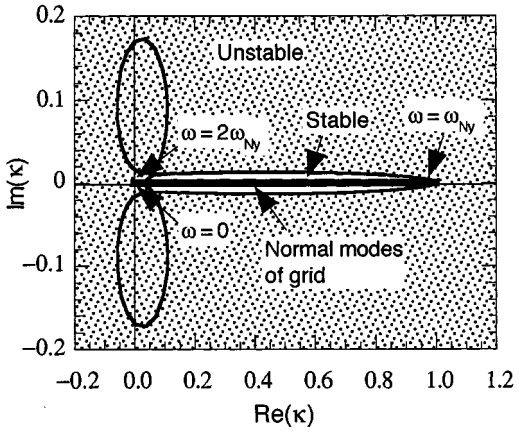

Fig. 3. Stability loop for the same Lorentz material as in Fig. 2, but with time step reduced to 0.7×10^{-17} s. All normal modes are stable.

However, the Nyquist requirement is not *sufficient* to ensure stability, as demonstrated by the Lorentz example in Fig. 2. In that example, $\mathrm{Im}[\hat{n}'^2(\omega)] > 0$ at low frequencies (Fig. 4) such that the stability loop is "folded" across the real $\hat{\kappa}^2$-axis and does not enclose any stable region. Stability requires that there exist a frequency ω_c, in the range $0 < \omega_c \leq \omega_{Ny}$ for

which $\mathrm{Im}[\hat{n}'^2(\omega)] \leq 0$ at all frequencies less than ω_c and also that $\hat{\kappa}^2(\omega_c) \geq 1$. For simple dispersive properties like those of the Debye material in Fig. 1, $\omega_c = \omega_{Ny}$, so this requirement is equivalent to the Nyquist requirement. However, for the Lorentz material in Figs. 2 and 4, a band of frequencies with $\mathrm{Im}[\hat{n}'^2(\omega)] > 0$ persists near $\omega = 0$, such that the normal modes with lowest $\hat{\kappa}^2$ are unstable until the time step is reduced below $\sim 0.7 \times 10^{-17}$ s.

A practical procedure to find the largest stable time step is to first compute Δ_{tNy}. If $\mathrm{Im}[\hat{n}'^2(\omega)] \leq 0$ for all $0 \leq \omega \leq \omega_{Ny}$ when Δ_{tNy} is used, then the largest stable time step is Δ_{tNy}. If not, then Δ_t should be reduced below Δ_{tNy} until the more general stability requirement in the previous paragraph is satisfied.

2) Stability for Anisotropic Materials: For anisotropic material properties, the situation is more complicated. In this case $\hat{\kappa}^2$ is not useful and we must deal directly with the numerical dispersion relation between ω and $\mathbf{k}$. Instead of each real ω mapping to a single *point* in the $\hat{\kappa}^2$-plane, as before, each real ω now maps to two polarization *surfaces* in $\mathbf{k}$-space. The transform of the real-ω line segment $0 \leq \omega \leq 2\omega_{Ny}$ is a solid region in $\mathbf{k}$-space instead of a loop. Stability requires that the rectangular block of $\mathbf{k}$-space containing the normal modes of the grid be fully contained within that stability region. To rigorously determine if a particular Δ_t is stable, we must evaluate the two solutions for ω at each of the normal modes of the grid and determine if any of the solutions have $\mathrm{Im}[\omega(\mathbf{k})] > 0$. Although somewhat laborious, this procedure will usually be faster than performing repeated FDTD runs to find a stable Δ_t.

D. Isotropic Nondispersive Lossy Dielectric

To compare with previous results, we compute the numerical dispersion relation and stability time step for an isotropic lossy dielectric with relative dielectric constant ε_r and conductivity σ. The continuous dispersion relation is

$$\mu_0\varepsilon_0\left(\varepsilon_r - \frac{j\sigma}{\varepsilon_0\omega}\right)\omega^2 = k^2. \tag{27}$$

In this case $\hat{\mu}'(\omega) = \hat{\mu}(\omega) = \mu_0$ and $\hat{\varepsilon}'(\omega) = \varepsilon_r - j\sigma g(\theta_t)/\omega$, so use of (11), (21), and (24) yields the numerical dispersion relations

$$\mu_0\varepsilon_0\left[\varepsilon_r\left(1 + \frac{\sigma\Delta_t}{2\varepsilon_0\varepsilon_r}\right) - \frac{j\sigma\Delta_t}{2\varepsilon_0\tan(\theta_t)}\right]\omega^2\,\mathrm{sinc}^2(\theta_t) = \sum_{\beta=x,y,z} k_\beta^2\,\mathrm{sinc}^2(\theta_\beta) \tag{28}$$

for the TF approach and

$$\mu_0\varepsilon_0\left[\varepsilon_r - \frac{j\sigma\Delta_t}{2\varepsilon_0\tan(\theta_t)}\right]\omega^2\,\mathrm{sinc}^2(\theta_t) = \sum_{\beta=x,y,z} k_\beta^2\,\mathrm{sinc}^2(\theta_\beta) \tag{29}$$

for the TA approach. Note that both forms converge to the continuous dispersion relation as $\Delta_x, \Delta_y, \Delta_z \to 0$ and $\Delta_t \to 0$, and that for lossless material they converge to the well-known dispersion relations [2], [3] . They are also in agreement with the results of Pereda *et al.* [6], except for the factor $(1+\sigma\Delta_t/2\varepsilon_0\varepsilon_r)$ in (28) versus $(1-\sigma\Delta_t/2\varepsilon_0\varepsilon_r)$ in Pereda *et al.*. Pereda confirms [14] that the factor should be $(1+\sigma\Delta_t/2\varepsilon_0\varepsilon_r)$.

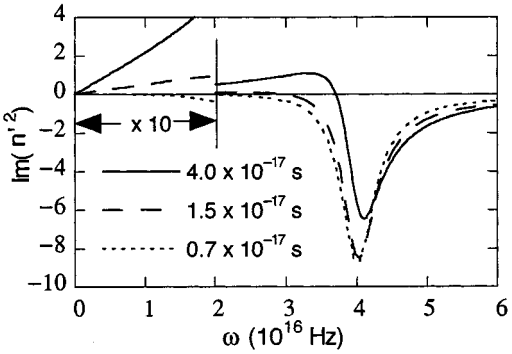

Fig. 4. $\mathrm{Im}[\hat{n}'^2(\omega)]$ for the same Lorentz material as in Figs. 2 and 3 for three values of Δ_t, including Nyquist value of 4.0×10^{-17} s. Positive $\mathrm{Im}[\hat{n}'^2(\omega)]$ at low frequencies for the larger two Δ_t indicates instability at these frequencies, so Δ_t must be reduced below 0.7×10^{-17} s for absolute stability.

We determine the maximum time step from the Nyquist stability requirement by substituting the Nyquist frequencies $\omega \to \pi/\Delta_t$ and $k_\beta \to \pi/\Delta_\beta$ into (28) and (29), yielding

$$\frac{\mu_0\varepsilon_0\varepsilon_r}{\Delta_t^2} = \sum_{\beta=x,y,z}\frac{1}{\Delta_\beta^2} \tag{30}$$

for the TA approach and

$$\mu_0\varepsilon_0\left(\varepsilon_r + \frac{\sigma\Delta_t}{2\varepsilon_0}\right)\frac{1}{\Delta_t^2} = \sum_{\beta=x,y,z}\frac{1}{\Delta_\beta^2} \tag{31}$$

for the TF approach. These results are also in agreement with Pereda *et al.*. The TA result is the same stability limit as for a lossless material with the same ε_r. In other words, σ has no effect on stability when the TA approach is used. On the other hand, the TF result implies a longer permissible time step than for a lossless material with the same ε_r.

E. Debye and Drude Dispersive Materials

If we treat a Drude material as a Debye material with nonzero conductivity [3], both materials have the continuous susceptibility function

$$\chi(\omega) = \frac{1}{1 + j\dfrac{\omega}{v_c}} \tag{32}$$

with

$$\hat{\varepsilon}(\omega) = \varepsilon_\infty + (\varepsilon_s - \varepsilon_\infty)\chi(\omega) \tag{33}$$

for the Debye material and

$$\hat{\varepsilon}(\omega) = \varepsilon_\infty - (\omega_p/v_c)^2\chi(\omega) + \frac{\sigma}{j\omega\varepsilon_0} \tag{34}$$

for the Drude material (with $\sigma = \varepsilon_0\omega_p^2/v_c$). The discrete susceptibility corresponding to (32) is [3]

$$\chi_m = \exp(-mv_c\Delta_t)[1 - \exp(-v_c\Delta_t)] \tag{35}$$

so that the numerical susceptibility from (15) is

$$\chi'(\omega) = \frac{1 - \exp(-v_c\Delta_t)}{1 - \exp[-(j\omega + v_c)\Delta_t]}. \tag{36}$$

The resultant numerical dispersion relation for the isotropic Debye material is

$$\mu_0\varepsilon_0 \left[\varepsilon_\infty + (\varepsilon_s - \varepsilon_\infty)\frac{1 - \exp(-v_c\Delta_t)}{1 - \exp[-(j\omega + v_c)\Delta_t]}\right] \omega^2 \operatorname{sinc}^2(\theta_t) = \sum_{\beta=x,y,z} k_\beta^2 \operatorname{sinc}^2(\theta_\beta). \tag{37}$$

The relation for the Drude material is

$$\mu_0\varepsilon_0 \left\{\varepsilon_\infty - (\omega_p/v_c)^2 \frac{1 - \exp(-v_c\Delta_t)}{1 - \exp[-(j\omega + v_c)\Delta_t]} + \frac{\omega_p^2\Delta_t}{2jv_c}\left[\frac{\cos(\theta_t)}{\operatorname{sinc}(\theta_t)}\right]\right\} \omega^2 \operatorname{sinc}^2(\theta_t) = \sum_{\beta=x,y,z} k_\beta^2 \operatorname{sinc}^2(\theta_\beta) \tag{38}$$

for the TF approach and

$$\mu_0\varepsilon_0 \left\{\varepsilon_\infty - (\omega_p/v_c)^2 \frac{1 - \exp(-v_c\Delta_t)}{1 - \exp[-(j\omega + v_c)\Delta_t]} + \frac{\omega_p^2\Delta_t}{2jv_c}\left[\frac{\exp(j\theta_t)}{\operatorname{sinc}(\theta_t)}\right]\right\} \omega^2 \operatorname{sinc}^2(\theta_t) \sum_{\beta=x,y,z} k_\beta^2 \operatorname{sinc}^2(\theta_\beta) \tag{39}$$

for the TA approach.

The maximum Nyquist time step can again be determined by substitution of the temporal and spatial Nyquist frequencies into (37)–(39). A numerical example is given in Section III-B.

F. Lorentz Dispersive Material

The continuous $\chi(\omega)$ for a second-order Lorentz material can be written as [3]

$$\chi(\omega) = \frac{(\varepsilon_s - \varepsilon_\infty)}{\omega_p^2 + 2j\omega\delta_p - \omega^2} = \frac{\gamma_p\beta_p}{(\alpha_p^2 + \beta_p^2) + 2j\omega\alpha_p - \omega^2} \tag{40}$$

where $\alpha_p = \delta_p, \beta_p = \sqrt{\omega_p^2 - \delta_p^2}$, and $\gamma_p = \omega_p^2(\varepsilon_s - \varepsilon_\infty)/\beta_p$. Furthermore, from [3, eq. (8.42)] we can identify the components of (14) as

$$v_c = \alpha_p - j\beta_p \tag{41}$$

and

$$\hat{G} = \frac{-j\gamma_p}{\alpha_p - j\beta_p}\{1 - \exp[-(\alpha_p - j\beta_p)\Delta_t]\} \tag{42}$$

so that (15) yields

$$\chi'(\omega) = -\frac{j\gamma_p}{2(\alpha_p - j\beta_p)}\left\{\frac{1 - \exp[-(\alpha_p - j\beta_p)\Delta_t]}{[1 - \exp[-(j\omega + \alpha_p - j\beta_p)\Delta_t]]} + \frac{1 - \exp[-(\alpha_p + j\beta_p)\Delta_t]}{[1 - \exp[-(j\omega + \alpha_p + j\beta_p)\Delta_t]]}\right\}. \tag{43}$$

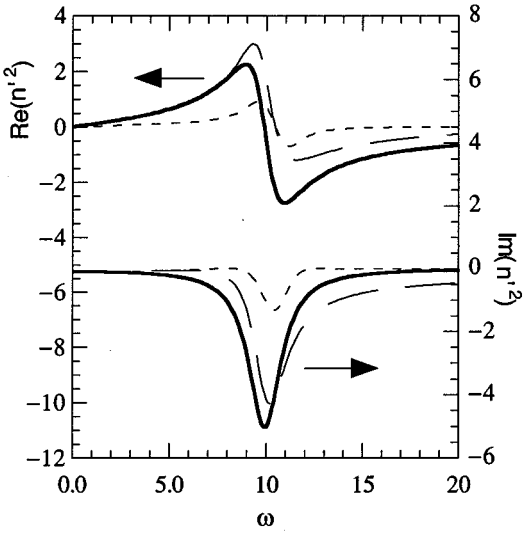

Fig. 5. Predicted numerical dispersion for Lorentz material with $\varepsilon_s = 1, \varepsilon_\infty = 0, \omega_p = 10, \delta_p = 1$, and $\Delta_x = 0.0001$. Time steps are $\delta_p\Delta_t = 0.0001$ (heavy lines), $\delta_p\Delta_t = 0.1$ (long-dashed lines), and $\delta_p\Delta_t = 0.3$ (short-dashed lines).

The dispersion relation and stability can then be determined straightforwardly as in the previous examples.

As an example, Fig. 5 shows the effective $\hat{n}'^2(\omega)$ for a 1-D Lorentz material with $\varepsilon_s = 1, \varepsilon_\infty = 0, \omega_p = 10$, and $\delta_p = 1$. A small spatial step corresponding to $k\Delta_x$ = 0.0001 was used to minimize spatial discretization effects and emphasize temporal effects. The time step Δ_t was varied to yield ratios of $\delta_p\Delta_t$ between 0.0001 and 0.3. The result shows that appreciable distortion occurs when $\delta_p\Delta_t \geq 0.03$.

III. Numerical Results

In this section, we compare the predicted dispersion and stability properties to those obtained from actual FDTD runs. The FDTD calculations were performed by custom code written either in MATLAB or FORTRAN. The examples include a comparison of numerical dispersion for a material that is both anisotropic and dispersive and evaluations of stability for isotropic Drude and Lorentz materials.

A. Dispersion for Anisotropic Dispersive Dielectric

To demonstrate the procedure with a material that is anisotropically dispersive, we modeled the situation shown in Fig. 6. A TM-polarized plane wave is incident from vacuum in the $y = 0$ plane at an angle of incidence from the normal θ_i. The material in the lower half-plane was assumed to have lossy dielectric properties in the z-direction with $\varepsilon_r = 2.0$ and $\sigma_z = 0.01$ siemens/m. In the x-direction, the material has lossy Debye dispersion with $\varepsilon_s = 2.0, \varepsilon_\infty = 1.0$, $v_c = 10^9$ Hz, and $\sigma_x = 0.01$ siemens/m. Periodic boundary conditions (BC's) were imposed at the sides of the space to simulate an infinite

interface. Perfectly matched layer (PML) BC's [2] were used at the top and bottom.

The incident plane wave generates both a reflected wave in vacuum and a decaying transmitted wave in the anisotropic material. We predicted the complex k_z for the transmitted wave and compared to the value obtained in FDTD runs. First consider the predicted value. The continuous dispersion relation for TM waves in the $y = 0$ plane in the material is determined by the solution of the determinant equation [13]

$$0 = \begin{vmatrix} \omega^2\mu_0\hat{\varepsilon}_x - k_z^2 & k_x k_z \\ k_x k_z & \omega^2\mu_0\hat{\varepsilon}_z - k_x^2 \end{vmatrix}. \tag{44}$$

Since k_x is preserved across the interface, it is easily computed from the free-space wavelength λ_0 as $k_x = (2\pi/\lambda_0)\cos(\theta_i)$. Then (44) becomes a polynomial equation that yields two values of k_z for each ω, representing forward and reverse solutions. To then determine the numerical dispersion relation, we simply substituted the modified σ', k', and $\chi'_{\text{Debye}}(\omega)$ into (44), and solved for k_z as a function of ω.

We determined "experimental" values for the complex k_z using a two-dimensional (2-D) FDTD calculation with the TF method. The cell size was 0.05 m in both directions. The time step was 1.1785×10^{-10} s. The FDTD problem was run until stability was obtained (5000 time steps), and then a Simplex method was used to determine k_z. Fig. 7 shows comparisons among the continuous, modeled, and FDTD values for $\theta_i = \pi/4$. Although the FDTD values differ from the continuous values by up to 10 percent, the FDTD and model differ by less than about 0.1% over the full range of wavelengths. This residual error is an upper limit to the actual error in the model, since it is comparable to the uncertainty in the fitting procedure used to extract the FDTD values.

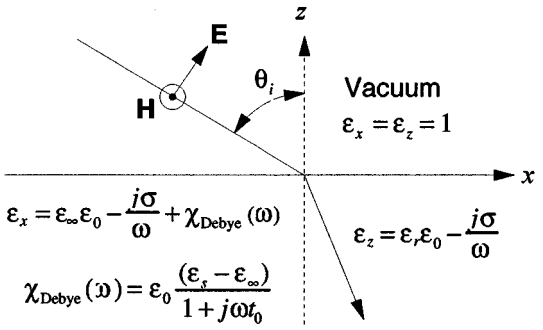

Fig. 6. Geometry for anisotropic dispersive experiment.

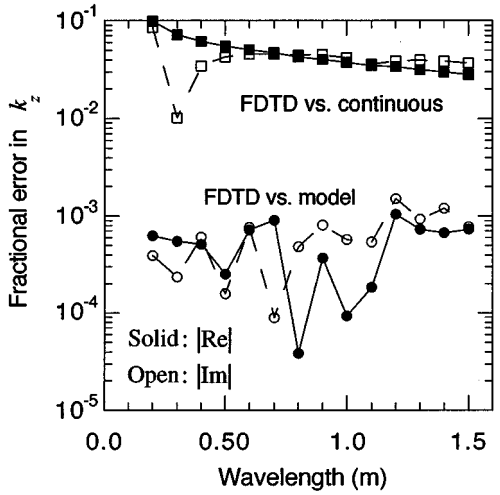

Fig. 7. Comparison of relative error in k_z for FDTD versus continuous and FDTD versus model in anisotropic situation shown in Fig. 6 with $\theta_i = \pi/4$. Residual difference between model and FDTD is less than 0.1%.

B. Stability with Drude Material

We next determined the maximum stable time step for a Drude material with isotropic properties $\omega_p = 4.1699 \times 10^{15}$ Hz and $v_c = 1.4373 \times 10^{15}$ Hz. A 2-D isotropic grid was used. The dispersion and stability analysis (with two dimensions) indicated that TF update equations would be stable in an analysis using the 3-D Courant time step Δ_{c3d}. The FDTD calculation was indeed stable. However, when TA update equations were used, analysis indicated that the problem would be unstable at Δ_{c3d} and require a time-step reduction that varied with the grid spacing, $\Delta_x = \Delta_y$. We then performed FDTD runs using time steps surrounding the predicted values. As shown in Table I, the agreement between predicted and achieved values was very good.

TABLE I
COMPARISON OF PREDICTED AND ACTUAL TIME STEP REDUCTION NEEDED FOR DRUDE MATERIAL ($\omega_p = 4.1699 \times 10^{15}$ Hz AND $v_c = 1.4373 \times 10^{15}$ Hz) USING TA UPDATE EQUATIONS

Grid Spacing $\Delta_x = \Delta_y$ (nm)	Time-step reduction		
	Predicted reduction required	Yielded stable FDTD	Yielded unstable FDTD
1.700	0.88608	0.8859	0.8861
15.07	0.39320	0.3931	0.3933
42.81	0.15957	0.1594	0.1595
78.65	0.08842	0.0883	0.0885

C. Stability with Lorentz Material

Finally, consider the stability of the previously discussed Lorentz material in Figs. 2–4. The Courant time step of 4.0×10^{-17} s is smaller than the Nyquist requirement. However, a further time step reduction to 0.7×10^{-17} s is required to satisfy $\text{Im}[\hat{n}'^2(\omega)] \leq 0$ for $0 \leq \omega \leq \omega_{Ny}$ and achieve absolute stability at all spatial frequencies.

To test the actual FDTD stability, we modeled a slab of the Lorentz material surrounded on both sides either by vacuum or by lossless dielectric. As expected, the problem was unstable at the Courant time step in all cases. The time step required to achieve stability decreased as the permittivity of the surrounding dielectric was increased and was always greater than the absolute stability time step mentioned above.

This behavior is apparently associated with formation of cavity modes inside the Lorentz slab. The spatial frequencies

at which $\mathrm{Im}[\hat{n}'^2(\omega)] > 0$ possess optical gain and *can* result in instability, depending on the overall structure surrounding the material. The situation is analogous to a laser in which oscillation depends both on gain and on the presence of a reflecting cavity.

IV. Conclusion

We have presented simple techniques for predicting numerical dispersion and stability in FDTD calculations involving possibly dispersive and anisotropic materials. The techniques are applicable to the common case of linear FDTD calculations that are second order in both space and time, use either the TA or TF approach to incorporate conductivity, and use discrete convolution to incorporate dispersion. To our knowledge, this is the first such general procedure for computing numerical dispersion and stability in the discrete-convolution FDTD method.

Numerical dispersion is calculated by a simple substitution into the continuous dispersion relation. Stability is then determined from the numerical dispersion relation. For isotropic material properties, one can easily evaluate stability by first finding the Nyquist time step and then, if necessary, reducing from that value until $\mathrm{Im}[\hat{n}'^2(\omega)] \leq 0$ for $0 \leq \omega \leq \omega_{Ny}$. For anisotropic material properties, the stability can still be evaluated, but requires evaluation of the multiple complex solutions for ω at each of the normal modes of the grid.

Excellent agreement was achieved between predicted and FDTD-computed numerical dispersion of an anisotropic, dispersive material, and stability of isotropic Drude and Lorentz materials.

Acknowledgment

The authors would like to thank R. Luebbers and D. Kelley for pointing out some of the previous work in this area.

References

[1] K. S. Yee, "Numerical solution of initial boundary value problems involving Maxwell's equations in isotropic media," *IEEE Trans. Antennas Propagat.*, vol. AP-14, pp. 302–307, 1966.
[2] A. Taflove, *Computational Electrodynamics: The Finite-Difference Time-Domain Method*. Boston, MA: Artech House, 1995.
[3] K. S. Kunz and R. J. Luebbers, *The Finite Difference Time Domain Method in Electromagnetics*. Boca Raton, FL: CRC, 1993.
[4] R. J. Luebbers and F. Hunsberger, "FDTD for Nth-order dispersive media," *IEEE Trans. Antennas Propagat.*, vol. 40, pp. 1297–1301, 1992.
[5] Remcom, XFDTD, www.remcominc.com, , Remcom, Inc., State College, PA, 1997.
[6] J. A. Pereda, O. Garcia, A. Vegas, and A. Prieto, "Numerical dispersion and stability analysis of the FDTD technique in lossy dielectrics," *IEEE Microwave Guided Lett.*, vol. 8, pp. 245–247, July 1998.
[7] S. A. Cummer, "An analysis of new and existing FDTD methods for isotropic cold plasma and a method for improving their accuracy," *IEEE Trans. Antennas Propagat.*, vol. 45, pp. 392–400, Mar. 1997.
[8] C. Hulse and K. André, "Dispersive models for the finite-difference time-domain method: Design, analysis, and implementation," *J. Opt. Soc. Amer. A*, vol. 11, pp. 1802–1811, 1994.
[9] P. G. Petropoulos, "Stability and phase error analysis of FD-TD in dispersive dielectrics," *IEEE Trans. Antennas Propagat.*, vol. 42, pp. 62–69, Jan. 1994.
[10] W. H. Weedon and C. M. Rappaport, "A general method for FDTD modeling of wave propagation in arbitrary frequency-dispersive media," *IEEE Trans. Antennas Propagat.*, vol. 45, pp. 401–410, Mar. 1997.
[11] J. L. Young, "A full finite difference time domain implementation for radio wave propagation in a plasma," *Radio Sci.*, vol. 29, pp. 1513–1522, 1994.
[12] ——, "On the dispersion errors related to (FD)2TD type schemes," *IEEE Trans. Microwave Theory Tech.*, vol. 43, pp. 1902–1910, Aug. 1995.
[13] P. Yeh, *Optical Waves in Layered Media*. New York: Wiley, 1988.
[14] J. A. Pereda, private communication, 1998.

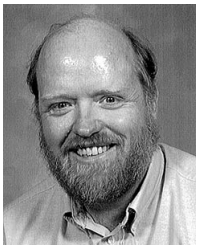

William A. Beck (M'99) received the B.S. degree in physics from Rensselaer Polytechnic Institute, Troy, NY, in 1974, and the M.S. and Ph.D. degrees in physics from the University of Maryland, College Park, in 1980 and 1986, respectively.

Since September 1995, he has been with the U.S. Army Research Laboratory, Adelphi, MD. His research interests include computational electromagnetics, device and system modeling for quantum well and thermal infrared detectors, and mobility spectrum analysis of magnetotransport measurements. From 1974 to 1995, he worked at Martin Marietta Laboratories, Baltimore, MD, on a variety of infrared detectors and materials.

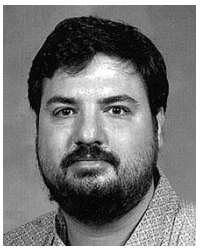

Mark Mirotznik was born in Sycamore, IL, in 1965. He received the B.E. degree from Bradley University, Peoria, IL, in 1988, and the M.S.E.E. and Ph.D. degrees from The University of Pennsylvania, Philadelphia, in 1991 and 1992, respectively.

Since September 1992, he has been with the Department of Electrical Engineering and Computer Science, The Catholic University of America, Washington, DC, as an Assistant Professor (1992–1998) and as an Associate Professor (1998–present). His research interests include computational electromagnetics with applications in the fields of biomedical engineering, diffractive optics, and infrared devices. He has been a member of the IEEE Committee on Radiation and Man and is currently an Associate Editor of the International Journal of Modeling and Simulation. In 1997 he was awarded the Distinguished Young Engineer Award from the Maryland Science Center.